Characteristics of few-mode fibre and its application in simultaneous strain and temperature measurement

IOP Conf. Series: Journal of Physics: Conf. Series **1065** (2018) 252005 doi:10.1088/1742-6596/1065/25/252005

Characteristics of few-mode fibre and its application in simultaneous strain and temperature measurement

Chenxu Lu[1,2], **Xiaopeng Dong**[1*], **Yunqing Guan**[1], **Juan Su**[1], **Tong Sun**[2] **and Kenneth T V Grattan**[2]

[1] Institute of Lightwave Technology, School of Information Science and Technology, Xiamen University, Xiamen, Fujian 361005, China.

[2] School of Mathematics, Computer Science and Engineering, City, University of London, Northampton Square, London, EC1V 0HB, UK

Abstract. This paper discusses a novel detection scheme to measure strain and temperature simultaneously using a section of specially designed few mode fibre (FMF). The work shows that the propagation constant difference between LP_{01} and LP_{02} modes, $\Delta\beta$, has a maximum at the critical wavelength (CWL) in the transmission spectrum. Theoretical analysis and experimental verification indicate that the peaks located on each side of the CWL shift to opposite directions under strain and temperature variations. The two peaks located closest to the CWL from both sides, Left Peak 1 and Right Peak 1, shift linearly with indeed different and high strain and temperature sensitivities, when an appropriate length of FMF is chosen, allowing such a device to be used to simultaneously measure strain and temperature over a known range.

1. Introduction

Optical fibre sensor devices to monitor strain and temperature simultaneously have been intensively studied because their potential applications in key industrial sectors. Typical methods based on using two fibre Bragg gratings (FBGs)[1] or Long Period Gratings (LPGs)[2] to make such a measurement use two individual sensors with different strain and temperature sensitivities, but these may cause errors as they are not located together. Monitoring two different interference fringes with different responses to strain and temperature is an alternative approach. Such a device then uses the transmission spectra of one single interferometer, for example constructed using a suspended core photonic crystal fibre [3], or a fibre taper and lateral-shifted junction [4] with single mode fibre (SMF). These devices typically are quite complex in terms of the signal analysis needed and interrogation processes required. An alternative and simpler sensor design is thus preferred and this is the approach used in this work, using a simple length of few mode fibre (FMF) as the basis of the device.

An in-line Mach-Zehnder Interferometer (MZI) is used where, based on the interference between the LP_{01} and LP_{02} modes, there is an identifiable critical wavelength (CWL) in the transmission spectra [5-7]. Such a device can be constructed as follows: a piece of few-mode fibre (FMF) is spliced between two pieces of SMF to create what is termed a SFS structure and in which the FMF supports only two modes, LP_{01} and LP_{02} [8], as a result of its design. The peaks on each side of the CWL shift in opposite directions, and with different sensitivities, under strain and temperature variations. This arises as the

[1] Corresponding author: Xiaopeng Dong (e-mail: xpd@xmu.edu.cn).

propagation constant differences of the LP_{01} and LP_{02} modes change non-monotonically with wavelength and reach a maximum at the CWL: further the sensitivities increase significantly when the peak wavelengths become close to the CWL. Therefore, by choosing the most appropriate length of FMF used, (in this case 20cm), the two peaks (Left Peak 1, Right Peak 1) closest to the CWL on each side, shift linearly in opposite directions with the maximum strain/temperature sensitivities. The SFS sensor designed in this way shows relatively high sensitivities, ease of identification and detection, and thus excellent simultaneous discrimination of strain and temperature.

2. Theoretical Analysis

The FMF cross section and relative refractive index difference profile (measured at a wavelength of 670nm) is shown in Fig. 1(a) and (b). The relative refractive index difference is defined as $\Delta n_{co/cli} = (n_{co/cli} - n_0)/n_0$, where $n_{co/cli}$ and n_0 are the refractive indices of core/i[th] inner cladding and pure silica of FMF, respectively.

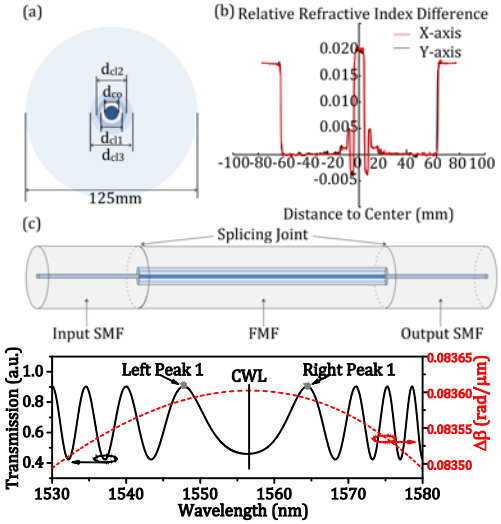

Figure 1. Structure of FMF and SFS. (a) Geometrical structure of FMF; (b) Relative refractive index difference profile of FMF measured at 670nm. The parameters used in the calculation are: d_{co}=8μm, Δn_{co}=1.99%, d_{cl1}=14.3μm, Δn_{cl1}=–0.40%, d_{cl2}=18μm, Δn_{cl2}=0.48%, d_{cl3}=30μm, Δn_{cl3}=0.14%. (c) Diagram of the SMF-FMF-SMF (SFS) structure.

Figure 2. Calculated Δβ vs. wavelength, simulated transmission spectrum of the SFS structure with straight unstrained 20cm FMF at a temperature of 25ºC.

Fig. 1 (c) illustrates the structure of the device designed. If the ratios of optical power transferred to the LP_{01} and LP_{02} modes in the FMF from the input SMF are t_{01} and t_{02}, respectively, the transmission, T, through the SFS structure is given by [9]:

$$T = P_{out} / P_{in} = t_{01}^2 + t_{02}^2 + 2t_{01}t_{02}\cos\left(\varphi(\lambda)\right) \quad (1)$$

where $\varphi(\lambda) = \Delta\beta(\lambda) \cdot L$ is the phase difference developed between the LP_{01} and LP_{02} mode in the FMF, of length L. Finite Element analysis is now used with these parameters and the simulated $\Delta\beta$ vs. wavelength relationship (at 25°C without axial strain) can be seen as a dashed line in Figure 2. The peaks closest to the CWL from the left and right sides are termed Left Peak 1 and Right Peak 1 (and these two peak wavelengths are represented as λ_{L1} and λ_{R1}, respectively).

2.1. Theoretical analysis on the strain and temperature sensitivities of peaks

The parameter $\varphi(\lambda)$ is a function of both the operational wavelength, λ, and the perturbation parameter, χ (temperature or strain). Across the sensing element (length L), the change of phase difference is written as is given in equation (2) [9]. If the FMF is strained longitudinally (at constant temperature) there is a change of length, ΔL, or the temperature increases ΔT at a constant strain, for a constant phase point ($\Delta\varphi = 0$), equation (2) can be written as equation (3) and (4), respectively.

$$\Delta\varphi = \frac{\partial\varphi}{\partial\lambda}\Delta\lambda + \frac{\partial\varphi}{\partial\chi}\Delta\chi \quad (2) \qquad \frac{\Delta\lambda}{\Delta\varepsilon} = -\frac{\partial\varphi}{\partial L}\left(\frac{\partial(\Delta\beta)}{\partial\lambda}\right)^{-1} \quad (3) \qquad \frac{\Delta\lambda}{\Delta T} = -\frac{1}{L}\left(\frac{\partial\varphi}{\partial T}\right)\left(\frac{\partial(\Delta\beta)}{\partial\lambda}\right)^{-1} \quad (4)$$

where $\Delta\varepsilon=\Delta L/L$ is the variation of axial strain. $\partial\varphi/\partial L$ and $\partial\varphi/\partial T$ are the change in phase difference produced by per unit increase in the actual length of the FMF, and. per degree change of temperature, respectively. The simulated strain and temperature sensitivity of peaks, $\Delta\lambda/\Delta\varepsilon$ and $\Delta\lambda/\Delta T$, vs. normalized wavelength (defined as λ/λ_{CWL}) can be seen as the solid line in Figure 3 (a) and (b), respectively.

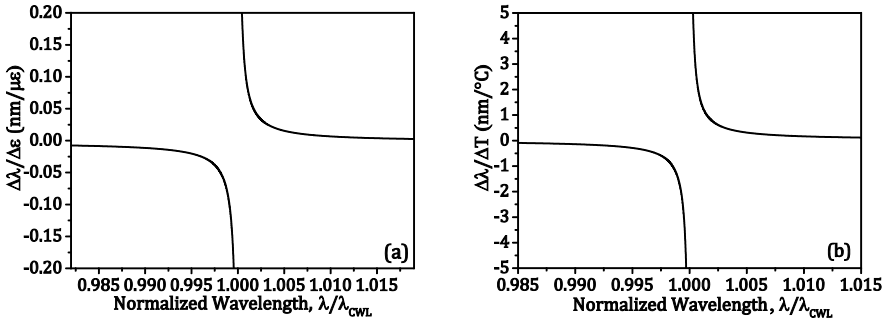

Figure 3. Simulated strain and temperature sensitivity of the SFS structure vs. the normalized wavelength: (a) strain sensitivity; (b) temperature sensitivity

2.2. Sensor matrix for simultaneous stain and temperature measurement

Assuming the axial strain and temperature sensitivities of Left Peak 1 and Right Peak 1 are $K_{\varepsilon L}$, K_{TL}, $K_{\varepsilon R}$, and K_{TR}, respectively, with an axial strain variation of $\Delta\varepsilon$ and a temperature variation of ΔT, the wavelength response of Left Peak 1, $\Delta\lambda_{L1}$, and Right Peak 1, $\Delta\lambda_{R1}$, the sensor matrix equation for simultaneous measurement of strain and temperature can be written as [10]:

$$\begin{pmatrix}\Delta\varepsilon\\ \Delta T\end{pmatrix}=\frac{1}{D}\begin{pmatrix}K_{TR} & -K_{TL}\\ -K_{\varepsilon R} & K_{\varepsilon L}\end{pmatrix}\begin{pmatrix}\Delta\lambda_{L1}\\ \Delta\lambda_{R1}\end{pmatrix} \tag{5}$$

where $D=\left|K_{\varepsilon L}K_{TR}-K_{TL}K_{\varepsilon R}\right|$ is the absolute value of the determinant of the coefficient matrix.

3. Experimental verification

The sensor scheme thus designed was set up and investigated (shown in Figure 4). The response of the SFS structure to axial strain was investigated, where the input SMF was fixed on a stage and the output SMF was spliced to a FBG (which has an axial strain sensitivity of 1.2pm/με). A similar axial strain was applied to both the FMF and FBG simultaneously, as the translation stage moves. Heat was applied to the FMF section using an electrically-controlled oven and the sensor transmission spectra were measured, in-line, using an Er-doped Amplified Spontaneous Emission (ASE) broadband light source and an Optical Spectrum Analyzer (OSA).

The sensing response of the SFS structure to strain and temperature individually was measured: for strain in the range from 0 to 600με at room temperature and, for temperature, over the range from 25.3ºC to 58ºC. As shown in Figure 5 and Figure 6, the Left Peak 1 shifts linearly to the blue and Right Peak 1 shifts linearly to the red as the axial strain/temperature increases. The measured strain sensitivities are -0.013nm/με and 0.009nm/με, and temperature sensitivities are -0.212nm/ºC and 0.262nm/ºC.

In order to verify the sensing scheme discussed using a measurement of the Left Peak 1 and Right Peak 1, simultaneous measurement of strain and temperature was undertaken, as shown in Figure 7. Here the temperature was controlled gradually to increase it from room temperature to about 60ºC (over 30 min) while a simultaneous strain of up to 200με was applied step-by-step (see Figure 7). Equation (5) enables the output response of the SFS sensor to be determined and this is plotted with the known applied values of strain and temperature respectively, in Figure 7 (b) and (c). Good agreement is seen, within a reasonable level of experimental error. Work is continuing to investigate the performance in more detail.

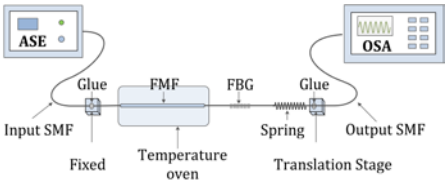

Figure 4. Experimental setup of the strain and temperature sensor based on the SFS structure.

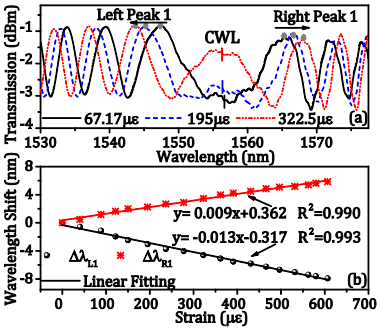

Figure 5. Transmission spectra of the SFS sensor (a) and wavelength shift of Left Peak 1 and Right Peak 1 (b) under axial strain.

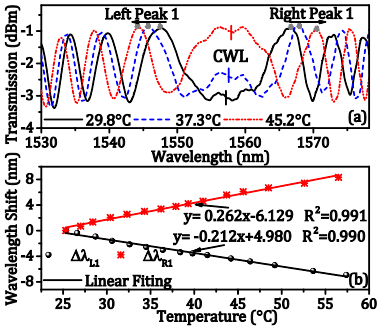

Figure 6. Transmission spectra of the SFS sensor (a) and wavelength shift of Left Peak 1 and Right Peak 1 (b) under temperature.

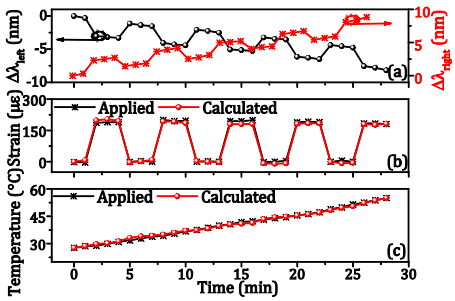

Figure 7. Results for simultaneous change of strain and temperature: (a) the values of $\Delta\lambda_{L1}$ and $\Delta\lambda_{R1}$ over the 30-minute; the applied and calculated strains (b) and temperatures (c).

4. Conclusion

This paper presents a comprehensive study on the strain and temperature sensitivities of the peaks in the transmission spectrum of an in-line MZI based on a special FMF. Both theoretical and experimental studies show that the strain and temperature sensitivities of peaks are governed by the wavelength spacing between the peak wavelengths and the CWL. A novel dual-parameter sensor was also developed based on the strain and temperature characteristics of the peaks, and the experimental results show that the proposed sensing scheme can simultaneously measure strain and temperature with a high sensitivity in a reasonable range of experimental errors.

5. References

[1] Sivanesan P, Sirkis J S,Murata Y, and Buckley S G 2002 *Opt. Eng.* **41** 2456
[2] Bey S K A K, Sun T, and Grattan K T V 2008 *Sens. Act. A* **144** 83
[3] Rota-Rodrigo S, López-Amo M, Kobelke J, Schuster K, Santos J L, and Frazão O 2015 *J. Lightw. Technol.* **33** 2468
[4] Lu P, and Chen Q 2010 *IEEE Photon. J.* **2** 942
[5] Su J, Dong X, and Lu C 2016 *IEEE J. Sel. Top. Quant.* **22** 4402307
[6] Su J, Dong X, and Lu C 2016 *IEEE Photon. Technol. Lett.* **28** 1387
[7] Lu C, Dong X, and Su J 2017 *J. Lightw. Technol.* **35** 2593
[8] Vengsarkar A M, and Walker K L 1991 *U. S. Patent* No. 5448674
[9] Salik E, Medrano M, Cohoon G, Miller J, Boyter C, and Koh J 2012 *IEEE Photon. Technol. Lett.* **24** 593
[10] Xu M G, Archambault J-L, Reekie L, and Dakin JP, 1994 *Electron. Lett.* **30** 108

Acknowledgments

This work was financially supported by National Natural Science Foundation of China (no. 61775186), Fujian Provincial Department of Science and Technology (Project no. 2014H6027); Marine and Fisheries Bureau of Xiamen (Project no. 16CZB025SF03). The support of the Royal Academy of Engineering and the George Daniels Educational Trust is greatly appreciated.